Journal of Hazardous Materials 445 (2023) 129899

Contents lists available at ScienceDirect

Journal of Hazardous Materials

journal homepage: www.elsevier.com/locate/jhazmat

Research Paper

Uptake and speciation of Zn and Pb by *Miscanthus* grown in contaminated soils

Innes Deans [a], Douglas I. Stewart [b], Jenny Jones [a], Jason Kam [c], Bhoopesh Mishra [a,d,*]

[a] School of Chemical and Process Engineering, University of Leeds, Leeds, United Kingdom
[b] School of Civil Engineering, University of Leeds, Leeds, United Kingdom
[c] Terravesta Ltd, Lincoln, United Kingdom
[d] Physics Department, Illinois Institute of Technology, Chicago, United States

HIGHLIGHTS

- Uptake of Zn and Pb by *Miscanthus* is proportional to their concentration in soil.
- Miscanthus shows higher compartmentalization of Zn in stem than in leaf.
- Loadings of Pb are higher for leaf than in stem.
- Zn is bound with S in leaves for nascent pot trial samples and to pectin/cell walls in the mature field trial samples.
- Zn bound to O/N ligands has primarily octahedral geometry in leaf which changes to tetrahedral geometry in stem.

GRAPHICAL ABSTRACT

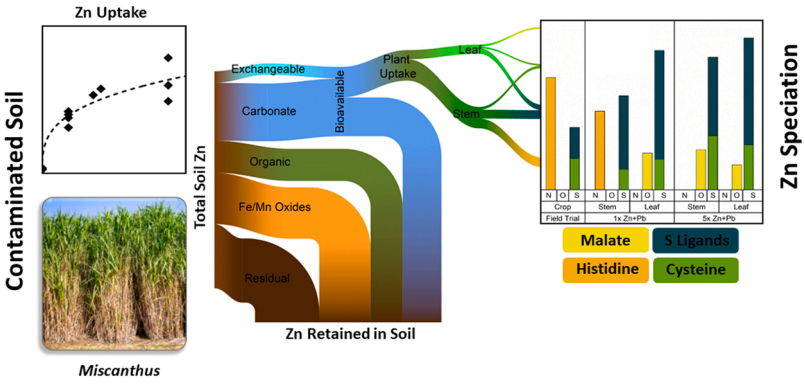

ARTICLE INFO

Editor: Guillaume Echevarria

Keywords:
Biomass
Metals uptake
Synchrotron
XANES
EXAFS

ABSTRACT

The uptake by and distribution of Zn and Pb within a novel seed-based *Miscanthus* hybrid grown in contaminated soil was assessed. Results from juvenile plants in a pot-trial was compared with data for mature biomass of the same species harvested during a field-trial. Both Zn and Pb uptake by juvenile plants were observed to increase in proportion to the soil concentrations. Both Zn and Pb accumulation differed between leaf and stem structures, and both were different in the mature biomass compared with juvenile plants. Analysis of X-Ray Absorption Fine Structures (XAFS) revealed different Zn speciation in stems and leaves, and differences in Zn speciation with plant maturity. Sulfur ligands consistent with the presence of cysteine rich metallothioneins (MT) and phytochelatin (PC) complexes were the dominant Zn species in juvenile plant leaves, together with octahedral O/N species typified by Zn-malate. Sulfur ligands were also prevalent in stems from juvenile plants, but predominant O/N speciation shifted towards tetrahedral coordination. In contrast, tetrahedral Zn coordination with O/N species predominated in the mature biomass crop. The XAFS spectra for the mature biomass were consistent with Zn being retained within cell walls as pectin and/or phosphate complexes.

* Corresponding author at: School of Chemical and Process Engineering, University of Leeds, Leeds, United Kingdom.
E-mail addresses: b.mishra@leeds.ac.uk, bmishra3@iit.edu (B. Mishra).

https://doi.org/10.1016/j.jhazmat.2022.129899
Received 1 February 2022; Received in revised form 22 August 2022; Accepted 31 August 2022
Available online 5 September 2022

1. Introduction

Miscanthus is a genus of perennial grass that includes species that have significant potential as feedstocks for the production of bioenergy. Hybrids such as *Miscanthus x giganteus* (Greef et al., 2001) have high biomass yields, low nutrient/fertiliser requirements and the ability to grow on marginal soils poorly suited to food crop production (Qin et al., 2011; Cadoux et al., 2012; Evans et al., 2015; Van Der Weijde et al., 2017). Research has also shown that some *Miscanthus* species can produce viable crops on land contaminated with Potentially Toxic Elements (PTEs) and offer potential for productive use of such lands for bioenergy crops (Kocoń and Jurga, 2017). However, some plant species can bioaccumulate PTEs when grown in contaminated soils, although the amount of uptake depends on the PTE, the degree of soil contamination, and the *Miscanthus* species/hybrid (Deng et al., 2004; Wanat et al., 2013; Li et al., 2014; Barbosa et al., 2015; Korzeniowska and Stanislawska-Glubiak, 2015; Krzyzak et al., 2017; Pidlisnyuk et al., 2019; Angelova and Zapryanova, 2021; Nsanganwimana et al., 2021; Al Souki et al., 2022).

The chemical composition of *Miscanthus* biomass displays seasonal variability which can be favourably manipulated to enhance combustion characteristics of the final biomass (Lewandowski and Heinz, 2003; Baxter et al., 2014). Research to date has focused on seasonal changes in the major inorganic species (N, S, Cl, K, Ca, Na, Fe, Mg). The major alkaline and earth metal concentrations are significantly lower within aerial (stem and leaf) structures when plants are senescent over winter than in other seasons and this results in changes in the fuel combustion characteristics (Baxter et al., 2012; Baxter et al., 2014). The extent to which *Miscanthus'* uptake of PTEs display such seasonal variations across the year is poorly understood in comparison.

Synchrotron X-ray techniques such as X-ray Absorption Fine Structure (XAFS) analyses are powerful tools which are increasingly finding application in the environmental and biological sciences. These techniques can be used to investigate PTE speciation in biological systems and provide insight into uptake and sequestration mechanisms within plants (Lombi and Susini, 2009; Zhao et al., 2014; Pushie et al., 2014; Adediran et al., 2015; Vijayan et al., 2015; Adediran et al., 2016a; Adele et al., 2018a, Cui et al., 2020). X-ray Absorption Near Edge Structures (XANES) can identify different species of a PTE, with high reproducibility between environmental samples, by comparing the position of the absorption edge and the variations in post-edge features with standard compounds (Castorina et al., 2019). PTE speciation can also be identified through Extended X-ray Absorption Fines Structure (EXAFS) analysis whereby the dominant biochemical ligands responsible for PTE sequestration can be distinguished (Mishra et al., 2010; Thomas et al., 2019; Mishra et al., 2020).

In Eudicot plants Zn has been found to be sequestered with several biochemical ligands, including tetrahedrally coordinated with N in Zn-histidine complexes (Salt et al., 1999; Kupper et al., 2004; Mishra et al., 2020), octahedrally coordinated with O-ligands in Zn-malate or Zn-citrate complexes (Sarret et al., 2002; Kupper et al., 2004; Mishra et al., 2020), tetrahedrally coordinated to S in Zn-cysteine complexes (Adele et al., 2018b; Mishra et al., 2020) and, in roots, in Zn-phytate complexes (Terzano et al., 2008; Adele et al., 2018a) where it is probably tetrahedrally coordinated to O (Rodrigues-Filho et al., 2005; Sarret et al., 2009; Neal et al., 2013). There is also evidence from eudicot plants that Zn speciation and localisation in the plants varies with the growth conditions and the amount of Zn available (Kelly et al., 2002; Adediran et al., 2016b; Adele et al., 2018a; Mishra et al., 2020). To date, fewer studies have investigated Zn speciation and localisation within grasses, such as *Miscanthus*, that are used as energy crops. Divergence during their evolution has led to major structural differences between both the leaves and stems of eudicot and monocot plants (Esau, 1977), so the distribution and speciation of Zn in grasses such as *Miscanthus* may differ.

In this study, a novel seed-based *Miscanthus* hybrid was grown in pot trials using soil with Zn and Pb contamination comparable with that at a polluted field site where a long-term field trial has been conducted (Krzyzak et al., 2017, Rusinowski et al., 2019b). The field trial identified the uptake of Zn and Pb, and to a lesser extent Cd, by *Miscanthus* plants. This study focusses on Zn and Pb due to their greater uptake. Bulk chemical analysis and XAFS techniques are used to determine Zn and Pb uptake and Zn speciation within juvenile plants in the pot trial. The results from the juvenile plants are compared with uptake and speciation observed within mature biomass from the same *Miscanthus* species harvested during the field trial. This study establishes patterns of uptake for these PTE, reveals significant differences in the pattern of storage within the plants, and identifies temporal and spatial changes in the biochemistry of Zn sequestration.

2. Materials and methods

2.1. Field Trial Biomass

A sample of *Miscanthus* was obtained from field trial at a PTE contaminated site at Bytom near Katowice (Poland). The plants were a novel seed-based hybrid developed by Aberystwyth University (UK) during the GIANT LINK Program (LK0863). The hybrid's growth performance characteristics under field trial conditions has been subjected to detailed analysis (Rusinowski et al., 2019b). The biomass material used in this study was mechanically harvested and shredded in March 2018 at the end of the winter senescence period in accordance with conventional agricultural practice.

2.2. Analysis of Soil

The soil from the field trial site has been described in literature and its chemical characteristics are summarised in Table 1. A random grab sample of the soil was obtained for this study, and its composition was confirmed as representative using a 50 kV/10 W Energy Dispersive X-ray Fluorescence (EDXRF) portable analyser (Olympus X-5000). The PTEs in the grab sample were characterised using an optimized Tessier procedure (Tessier et al., 1979; Rauret et al., 1989) which partitions them into five fractions: exchangeable; bound to carbonates; bound to Fe-Mn oxides; bound to organic matter; and residual (detailed protocol in the S.I. section1).

The Zn and Pb concentrations within each extraction were determined using an Agilent 2000 Atomic Absorption Spectrophotometer (AAS) operated with an air/acetylene flame and lamps/detector wavelengths of 213.9 nm and 217.0 nm were adopted for Zn and Pb respectively. The outcome of this preparatory investigation into the of Zn and Pb extractions is shown in Table 2.

Soil from Spen Farm, Yorkshire, UK (53°51'39.8"N 1°20'39.7"W) was collected for formulation of growing media within the pot trials (described below). The major chemical characteristics of the Spen Farm soil are reported in Table 1 and the results of Tessier extraction for Zn

Table 1
Major elemental analysis of soil from the Bytom field trial and the Spen Farm soil used for the pot trial.

Determinand	Units	Bytom Soil[1]	Spen Farm Soil
pH		7.3	7.6
Cation exchange capacity	meq/100 g	13.0	18.7
Ca	$mg/kg_{(dm)}$	1370	1780
P	$mg/kg_{(dm)}$	27	20
K	$mg/kg_{(dm)}$	23	106
Mg	$mg/kg_{(dm)}$	123	499
Na	$mg/kg_{(dm)}$	6	8
Total nitrogen	% w/w	0.2	0.16
Organic matter	% w/w	6.4	2.8

References:
[1] (Terravesta, 2018)
[2] (NRM, 2017)

and Pb are reported in Table 3.

2.3. Experimental Soil

To create a contaminated soil with Zn and Pb present in species comparable to those measured by Tessier extractions of the Bytom soil, $ZnCl_2$ and $PbCl_2$ (exchangeable) and $ZnCO_3$ and $PbCO_3$ (carbonate) were added to Spen Farm soil. The soil which replicated the Zn and Pb concentrations in the exchangeable and carbonate fractions of Bytom soil is subsequently referred to as 1x(Zn+Pb). Other contaminated soils were created using Zn only, Pb only, and both Zn and Pb using concentrations equivalent to 2x and 5x the concentrations in Bytom soil. In each case the proportion of the metal added as a chloride or carbonate salt was the same as the exchangeable/carbonate ratio for that metal observed in Bytom soil. Spen Farm soil was used without metal addition as the 'Control' soil. The metal concentrations added to the Spen Farm soil in the various pot experiments are shown in Table 4, along with the number of replicates for each growth condition.

2.4. Pot trial conditions

Three month old *Miscanthus* plants were supplied by Terravesta Ltd. (UK) in small pot ('plug') trays. The plants were grown from seed at Bell Brothers Nurseries Ltd., Boston (UK). The pot trial was conducted in a 4 × 5 m controlled environment plant growth suite at University of Leeds (UK). The growth suite was equipped with lighting on a timer to maintain a consistent 18-hour photoperiod each day. Photosynthetically active radiation (PAR) at the growing trays was monitored and observed in the range of 350 – 234 μmol m^{-2} s^{-1} with average being 281 μmol m^{-2} s^{-1}. A forced ventilation system maintained ambient O_2/CO_2 concentrations. Temperatures were controlled within the range of 30.8 – 18.7 ℃ with the mean temperature being 21.7 ℃. Each plant was grown in separate 0.25 L pots and were hand-watered every other day with tap water until saturated. The pot trial was run for 66 days (S.I. Figure S1).

2.5. Harvesting and sample preparation

Plants from the pot trial were individually harvested and divided into root, stem and leaf sections for each plant before being frozen at − 20℃. Biomass from the Bytom field trial was mechanically harvested and shredded (mixed stem and leaf material) on site consistent with standard agricultural practice before further size reduction and homogenisation using a Retsch SM300 Cutting Mill to particle size < 5 mm. Samples were prepared for chemical and XAFS analysis using standard drying and milling techniques (Luo et al., 2018; Li et al., 2019; Medas et al., 2019), as follows:. Each sample was weighed, dried at 105℃ for 4 h and weighed again to determine the moisture content and amount of dry matter. The samples for acid digestion and XAFS analysis were then ground to a fine powder using a Retch Cryo-mill using a zirconium oxide grinding jar which was cryogenically cooled using liquid nitrogen.

Table 3
Zn and Pb Tessier extractions of the Spen Farm soil.

Extraction Species	n	Zinc Range mg/kg (dm)	Zinc Mean mg/kg (dm)	Zinc %	Lead Range mg/kg (dm)	Lead Mean mg/kg (dm)	Lead %
i) Exchangeable	3	<LOD	0	0%	<LOD	0	0%
ii) Bound to Carbonates	3	<LOD	0	0%	<LOD	0	0%
iii) Bound to Fe & Mn Oxides	3	<LOD	0	0%	20–40	33	89%
iv) Bound to Organic Matter	3	<LOD	0	0%	<LOD	0	0%
v) Residual	3	70–76	73	100%	0–19	4	11%
Total		**70 – 76**	**73**	**100%**	**35–39**	**37**	**100%**

Table 4
Concentrations of metal species added to Spen Farm soil in the pot trials.

Sample ID	(n)	Zinc (mg (Zn)/kg (dm)) as $ZnCl_2$	Zinc as $ZnCO_3$	Zinc Total Zn	Lead (mg (Pb)/kg (dm)) as $PbCl_2$	Lead as $PbCO_3$	Lead Total Pb
Control	11	–	–	–	–	–	–
1x (Zn+Pb)	11	242	946	1188	75	469	544
High Zn							
2xZn	4	497	2162	2659	–	–	–
5xZn	4	1007	4693	5700	–	–	–
High Pb							
2xPb	4	–	–	–	172	1072	1244
5xPb	4	–	–	–	298	2249	2547
High Zn & Pb							
2x(Zn + Pb)	4	432	1877	2309	149	931	1080
5x(Zn + Pb)	4	1007	4693	5700	298	2249	2547

2.6. Analysis of biomass metal concentration

The PTE concentrations in both stem and leaf biomass was determined for approximately half of the replicates for each pot trial configuration (stem and leaf biomass from the remaining replicates were retained for XAFS analysis).

Acid digestion: Cryo-milled plant material (0.5 g) was added 10 mL of HNO_3 69% in a 250 mL flask and heated on a hot plate to achieve a strong effervescence. Once brown fumes had subsided (~4 h) the flasks were allowed to cool and 4 mL of 30% H_2O_2 added carefully before reheating for a further 2 h. Digested samples were allowed to cool overnight, made-up to 25 mL with ultra-pure dH_2O, and then filtered using a 0.2 μm Luer syringe filter.

ICP-MS analysis: The digestate was analysed using a Perkin Elmer Elan ICP-MS that had been previously calibrated for Zn and Pb using

Table 2
Zn and Pb Tessier extractions of the Bytom soil.

Extraction Species	n	Zinc Range mg/kg (dm)	Zinc Mean mg/kg (dm)	Zinc %	Lead Range mg/kg (dm)	Lead Mean mg/kg (dm)	Lead %
i) Exchangeable	3	240–168	197	5%	64–40	51	3%
ii) Bound to Carbonates	3	968–904	931	23%	456–432	443	24%
iii) Bound to Fe & Mn Oxides	3	1180–1120	1153	29%	100–80	87	5%
iv) Bound to Organic Matter	3	506–366	448	11%	812–336	647	35%
v) Residual	3	1168–1360	1277	32%	443–939	632	34%
Total		**3923–4115**	**4006**	**100%**	**1552–2048**	**1860**	**100%**

solution standards which had been matrix-matched for Si, Ca, Mg and K to concentrations consistent with that expected for *Miscanthus* based upon literature database values (ECN, 2018).

2.7. XAFS analysis

XAFS data across the Zn K-edge were collected from the biomass samples at beamline 10-BM-B at the Advanced Photon Source (APS), Chicago (USA). A Si(111) monochromator with an energy resolution of 1×10^{-4} ΔE/E was used, and the spectra were recorded in fluorescence mode using an ion chamber in Stern-Heald geometry. The ion chamber used to measure the I_0 was flooded with a mixture of 30% N_2 and 70% He gas. Biomass samples were pressed into 3 mm thick pellets and mounted using Kapton tape in an acrylic sample holder set at 45° to the beam. Energy grid alignment was facilitated by placing a Zn reference foil between I_t and I_{ref} detectors and these ion chambers were flooded with a mixture of 50% N_2 and 50% Ar gas.

A value of 9665 eV was selected as being just after the anticipated absorption edge associated with the Zn *K*-edge (see Fig. 2a). Scans were performed using 5 energy regions each of which start at − 150, − 30, + 60, + 6k, and + 9k eV above/below this value, finishing at + 12 keV, with energy step intervals for each region being 5, 0.4, 0.05k, 0.07k and 0.1k eV respectively. Thus greatest precision was achieved across the absorption edge, whilst conserving experimental time by allocating less time to data acquisition in other parts of the spectrum. Five consecutive scans were collected from each sample and the data was subsequently merged prior to analysis.

XANES data processing, including the alignment of spectra, background removal and Linear Combination Fitting (LCF) was performed using Athena software (Ravel and Newville, 2005). XANES spectra from the biomass samples were initially compared with 10 published reference spectra (see S.I. table S1) before the LCF analysis was conducted using spectra for aqueous solutions of Zn-malate, Zn-cysteine and Zn-histidine; and ZnS in powdered form (Mishra et al., 2020). The fitting range used was from − 30 to + 70 eV below/above E_0 of the sample, variable weights assigned to spectra were constrained to between 0 and 1. The sum of the weights used for each fit was not constrained.

EXAFS analysis was performed using Artemis (Demeter v.0.9.26) package of software (Ravel and Newville, 2005). Initial work was conducted using crystallographic data for Zn standard compounds (CIF files) along with Demeter's Ifeffit to fit EXAFS spectra to a range of Zn reference compounds: Zn-malate; Zn-histidine; Zn-cysteine; and ZnS. Spectral fitting was conducted for O/N, S and C scattering paths between 1.2 and 2.7 Å. These fitting parameters for the standards were then used as initial guess parameters for modelling EXAF of the biomass samples.

3. Results

3.1. Long-term Zn and Pb uptake by the Bytom Biomass

The Bytom soil contained mean concentrations for Total Zn and Total Pb of ~4000 and 1900 mg/$kg_{(dm)}$, respectively, which are ~10x and ~4x the thresholds at which soil is usually considered contaminated (Table 5). Biomass from the same seed-based hybrid grown at Bytom contained mean Zn and Pb concentrations of 93.7 and 14.4 mg/$kg_{(dm)}$, respectively, which are 6x and 7x typical values for *Miscanthus* plants grown in uncontaminated soil reported in the ECN database, and at levels close to, or in excess of, typical biomass fuel standards e.g. ISO 17225–7 (CEN, 2014).

3.2. Zn and Pb uptake by plants in the short-term pot trial

In the pot trials with the control soil the mean Zn concentrations in stem and leaf structures were 36 and 14 mg/$kg_{(dm)}$, respectively. Compared with the Zn concentrations for *Miscanthus* plants grown in uncontaminated soil these values were marginally above (stem) and at the lower end (leaf) of the typical range (Table 5).

Similarly, the mean Pb concentrations was below detection limit and 0.4 mg/$kg_{(dm)}$ in stem and leaf structures respectively, which were at the low end of the typical range for Pb concentrations for *Miscanthus* plants grown in uncontaminated soil. The concentrations of both Zn and Pb in biomass from the pot trial plants increased with the amount of that metal added to the Spen Farm soil. The data show that Zn concentration in the stem exceeds that in the leaves, but in contrast the Pb concentration in the stem was lower than in the leaves (Fig. 1).

The soil of the 1x(Zn+Pb) pot trial was engineered to replicate the contamination observed at the Bytom field site. However, the Zn concentrations in the plant stems and leaves were 387 mg/$kg_{(dm)}$ and 111 mg/$kg_{(dm)}$ respectively (n = 5). This was higher than that observed in the Bytom crop, which was predominantly stem material, that contained 94 mg/$kg_{(dm)}$ of Zn. In contrast, the Pb concentrations in the pot trial plants stems (1.4 mg/$kg_{(dm)}$) and leaves (3.6 mg/$kg_{(dm)}$) were

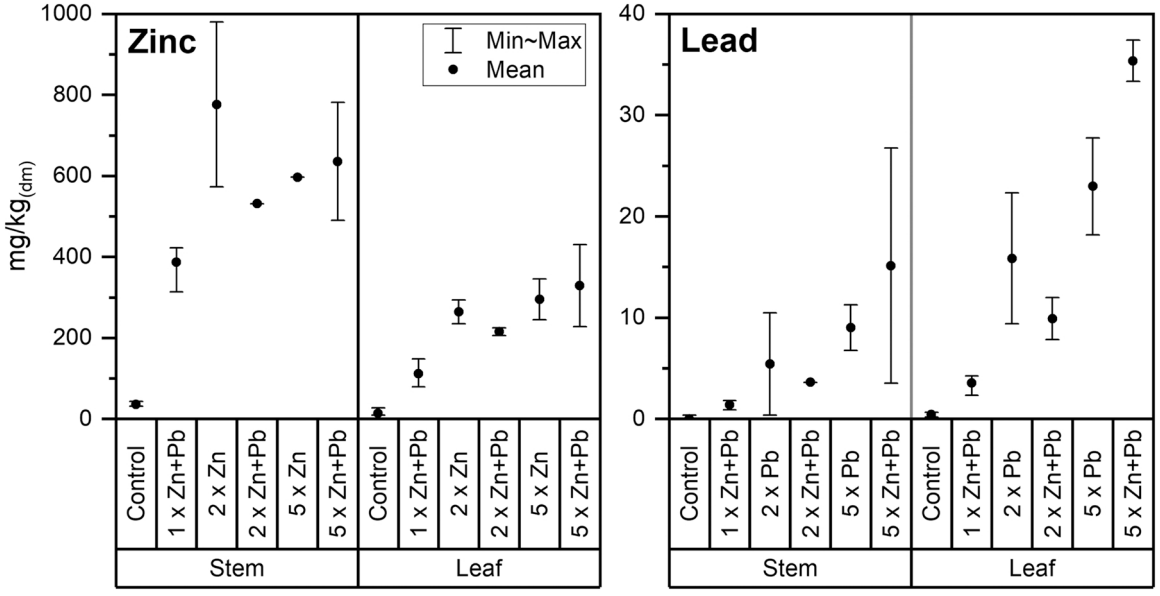

Fig. 1. Bulk Zn and Pb concentrations in stem and leaf materials across soil conditions adopted in the pot trial.

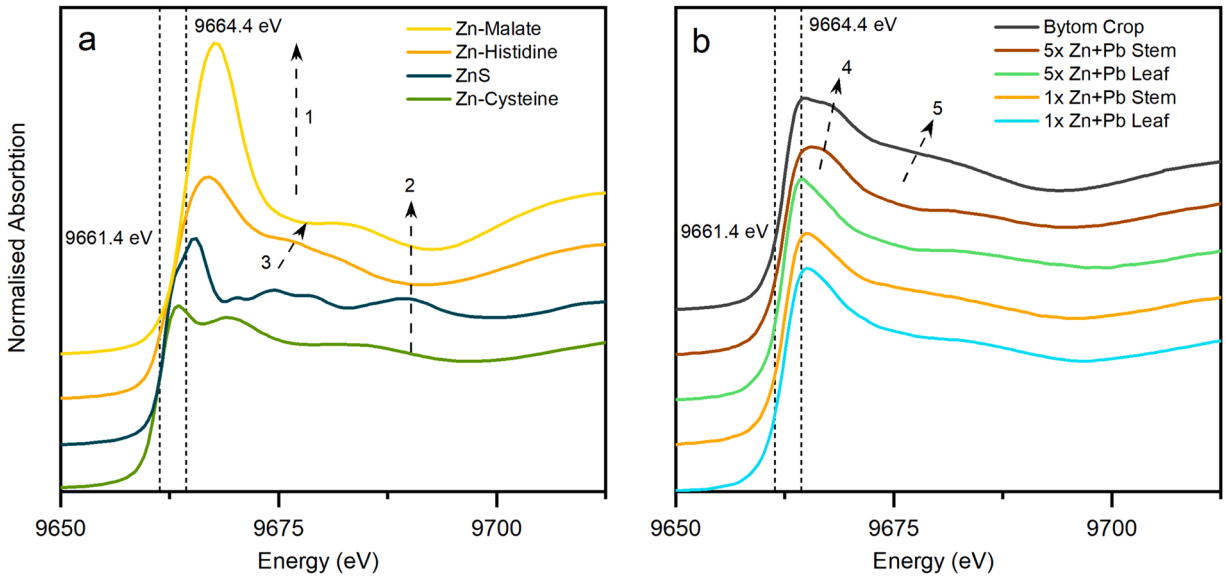

Fig. 2. Zn XANES spectra for: (a) Zn standard compounds (Mishra et al., 2020); (b) biomass samples. Absorption edge energies are shown for Zn-cysteine (9661.4 eV) and Zn-malate (9664.4 eV).

Table 5
Comparison of PTE concentration in Bytom soil and biomass compared with uncontaminated *Miscanthus* and example threshold values for defining contaminated soils.

	Soil Comparison		Biomass Comparison		
	Dutch Std. Intervention Value[1]	Bytom Soil	'Typical' *Miscanthus*[2]	Bytom Biomass	ISO 17225–7 (Class B)[3]
Contaminant	Threshold mg/kg (dm)	Mean mg/kg (dm)	Mean (Range) mg/kg (dm)	Mean (Range) mg/kg (dm)	Threshold mg/kg (dm)
Zn	350	4006	16 (9 – 33)	94 (60 – 116)	≤ 100
Pb	530	1859	2 (0 – 10)	14 (13 – 16)	≤ 0.1

References:
[1] NOAA (2008)
[2] ECN (2018)
[3] BSI (2020)

substantially lower than in the Bytom crop (14.4 mg/kg$_{(dm)}$).

3.3. XAFS results

The XANES spectra for biomass samples possess a Zn absorption edge that varied between 9662.4 and 9662.6 eV (Fig. 2b). These values were towards the lower end of the energy range observed for Zn standard compounds (Fig. 2a; (Mishra et al., 2020)) and were consistent with the presence of S coordinated species as the absorption edges were below even tetrahedral O/N coordinated Zn species (e.g. Zn-histidine at 9663.4 eV).

The magnitude of the Fourier Transform (FT) of the Zn EXAFS spectra for the Bytom field trial biomass exhibit first peaks at 1.53 Å, whereas the stem material from the 5x(Zn+Pb) pot trial has a first peak at 1.66 Å, the leaf material from the 5x(Zn+Pb) pot trial has a first peak at 1.75 Å (Fig. 4c). These values differ from the FT of the EXAFS spectra for the Zn-histidine and Zn-malate standards which have peaks at 1.51 Å and 1.58 Å, respectively (O/N coordination of Zn), while the S coordinated Zn-cysteine and Zn-sulfide standards both have peaks at 1.85 Å (Fig. 4a; (Mishra et al., 2020)). The S coordinated species also display characteristic spectral features in the real part of the EXAFS FT at around 2.1 – 2.2 Å which differentiate them from O/N species (Fig. 4b). The magnitude plot of the FT from the powdered ZnS standard also displayed significant peak(s) at 3 – 4 Å, which was characteristic of strong multiple scattering pathways associated with Zn in the second coordination shell. The other standards were aqueous solutions, so backscattering from the second coordination shell was not seen. Differences between the spectra

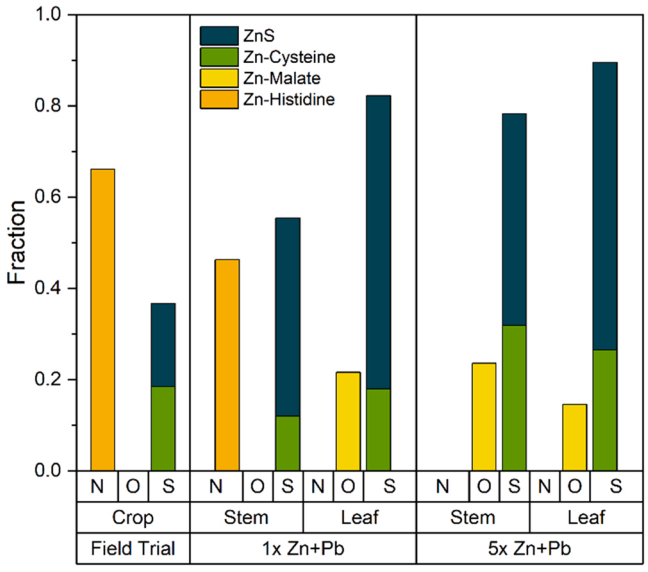

Fig. 3. results of LCF of the relative weight for Zn species in Miscanthus from the Bytom Field Trial and the Growth Trial plant sections.

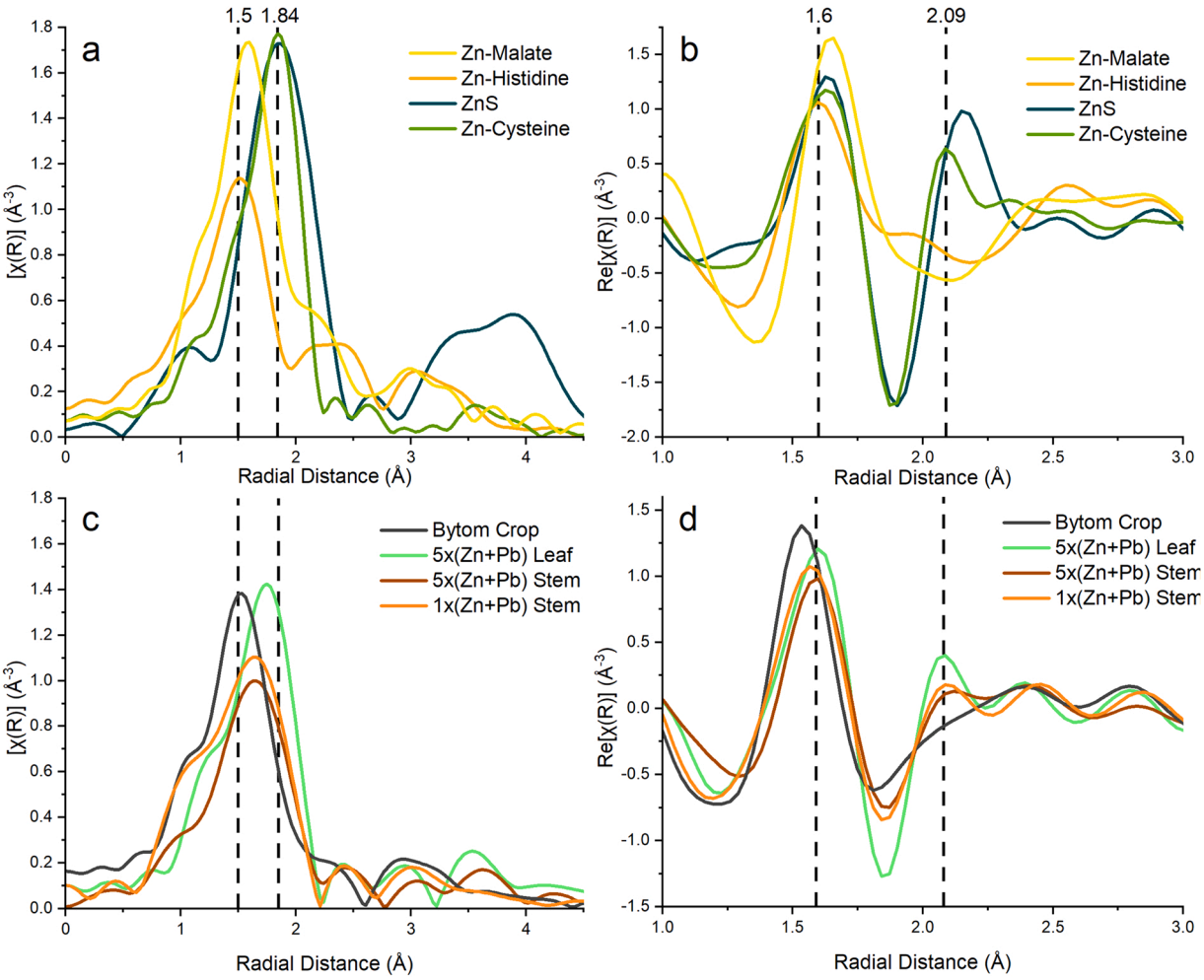

Fig. 4. Fourier Transformed of EXAFS: (a) magnitude $|\chi(R)|$ for Zn standards; (b) magnitude $|\chi(R)|$ for *Miscanthus* samples; (c) Real part $\mathrm{Re}|\chi(R)|$ for Zn standards; (d) Real part $\mathrm{Re}|\chi(R)|$ for *Miscanthus* samples.

for Zn-histidine and Zn-malate standards are less pronounced, but the most significant was observed in the first peak of the magnitude of the EXAFS FT, where the tetrahedral structure of histidine resulted in a lower peak of the magnitude of the EXAFS FT when compared with octahedral structure of malate (Fig. 4a).

3.4. Linear combination fitting of XANES

Linear combination fitting (LCF) of XANES from the biomass samples has been undertaken using the spectra for the Zn-histidine, Zn-malate, Zn-cysteine, and ZnS standards. These four standard compounds were chosen as characteristic compounds for the range of bonding environments anticipated for Zn in biomass. In Zn-cysteine and Zn-histidine the Zn is tetrahedrally coordinated to S or N respectively within an organic compound. Whereas, in Zn-malate the Zn is octahedrally coordinated to O (Mishra et al., 2020). The Zn within ZnS is tetrahedrally coordinated with S within an inorganic compound (Kisi and Elcombe, 1989). The energy of the inflection point of the Zn K-edge associated with these standards increases in the order: Zn-cysteine (9661.4 eV), ZnS (9661.9 eV), Zn-histidine (9663.4 eV), and Zn-malate (9664.4 eV) (Fig. 2a). Further spectral features differ between the standards. The octahedral O coordination of Zn-malate produces a distinctly higher and more tapered white line (arrow 1), O and N coordinated Zn-malate and Zn-histidine display spectral features around 9690 eV which are absent or opposed in S-coordinated species (arrow 2), whilst Zn-histidine can be differentiated by a shoulder (arrow 3) in the post-edge region of ~9675 eV (Mishra et al., 2020).

LCF for leaf material from the pot trials (Fig. 3 and S.I. Figure S2) suggests Zn coordination was similar in both the 5x(Zn+Pb) and 1x (Zn+Pb) pot experiments, with best fit achieved with ~80% weighting on S species (ZnS and Zn-cysteine) with the remainder being O species (Zn-malate). In comparison, LCF of stem material from the pot trials suggests that the amount of Zn uptake affects the coordination environment of Zn with predominantly S-coordination in stem material from the 5x(Zn+Pb) pot experiment, but more equal amounts of S and N coordination in stem material from the 1x(Zn+Pb) experiment. The biomass from the Bytom field trial comprised mostly of stem material. In this material N species contributed about 2/3rd of the signal and S species contributed the remaining 1/3rd of the XANES signal.

3.5. Qualitative analysis of EXAFS

The Bytom Crop, 1x(Zn+Pb) stem sample, and the 5x(Zn+Pb) stem and leaf samples provided sufficient signal to noise ratio to enable analysis of EXAFS spectra (noise in the data prevented EXAFS analysis for the 1x(Zn+Pb) leaf sample). Comparing plots of the Fourier Transforms (FT) for these spectra against those obtained for Zn-standard compounds (Mishra et al., 2020) enabled a qualitative analysis of the Zn ligands within the Bytom and pot trial samples (Fig. 4).

The magnitude of the FT for the samples (Fig. 4c) highlighted differences in the position of the first peaks indicating changes in Zn coordination environments. The shortest radial distance was associated

with the Bytom crop (1.53 Å), followed by increasing peak position distances for the 1x(Zn+Pb) stem (1.63 Å), 5x(Zn+Pb) stem (1.66 Å) and leaf material (1.75 Å). All these phase uncorrected peak positions occur within the range of values associated with the of Zn standard compounds (Fig. 4a). Zn standards exhibit increasing radial distance as follows: Zn-histidine (1.50 Å), Zn-malate (1.60 Å), with both Zn-cysteine and ZnS having the same peak position (1.84 Å). The first peak of the 5x(Zn+Pb) leaf sample was much closer to the radial distance associated with S-coordinated species than the other samples. Stem samples from the pot trials demonstrate similar peak positions, i.e. 1.63 Å and 1.66 Å for samples 1x(Zn+Pb) and 5x(Zn+Pb) respectively. Peak position in the range of 1.63–1.66 Å suggest a mixed coordination environment with higher O/N contribution. In contrast, the peak position for the Bytom crop (1.53 Å) was similar to that of the Zn-histidine standard.

The real part of the FT spectra for the Zn standards (Fig. 4b) illustrate significant spectral features for the S-coordinated species (ZnS and Zn-cysteine) with characteristic peaks at radial distances 2.09 Å and 2.15 Å, respectively. These features are not observed in the FT spectra for the O/N coordinated Zn-histidine or Zn-malate standards and so it can be used to identify the presence of S-species. The real part of the FT spectra for the biomass samples demonstrates this characteristic feature to different extents (Fig. 4d). The 5x(Zn+Pb) leaf sample demonstrates a clear peak at 2.09 Å, which is consistent with the presence of Zn-cysteine. Smaller peaks at the same radial distance were observed in both 1x(Zn+Pb) and 5x(Zn+Pb) stem samples from the pot trials; however, the signal was weaker suggesting cysteine ligation was less prevalent. There was no clear indication of S species being present in the Bytom crop sample as the real part of its FT does not demonstrate the characteristic features around 2.09 – 2.15 Å.

3.6. Quantitative modelling of EXAFS

In order to quantify Zn coordination environment in the biomass samples, a shell-by-shell fitting approach was used for quantitative modelling of the EXAFS data (Table 6 and Supplementary Information Figure S2). A low signal to noise ratio for the leaf material from the 1x (Zn+Pb) pot trial sample, which has the lowest Zn concentration of all the samples, rendered that data unsuitable for quantitative modelling with satisfactory statistical parameters (Fig. 1).

The first shell of the Bytom field trail biomass sample was best fit with coordination numbers of 0.7 (± 0.1) S and 3.4 (± 0.1) O/N at distances 2.27 (± 0.01) and 1.99 (± 0.01) Å, respectively. The stem material of the 1x(Zn+Pb) pot trial sample produced similar results within error. Best fit values for the first shell of the 1x(Zn+Pb) data were 0.8 (± 0.1) S and 3.5 (± 0.4) O/N at distances 2.30 (± 0.01) Å and 1.99 (± 0.01) Å respectively. The fit for 5x(Zn+Pb) stem sample was also comparable with the previous samples, with 0.8 (± 0.6) S and 3.4 (± 0.7) O/N at distances of 2.29 (± 0.01) Å and 2.06 (± 0.02) Å respectively. In each of these three samples the overall sum of coordination numbers for the first shell was just over 4 which suggests a predominantly tetrahedral coordination environment.

Table 6
EXAFS fitting parameters for biomass samples.

Sample	Path	CN	R (Å)	σ^2 (Å^2)
Bytom CROP	S	0.7 (± 0.1)	2.27 (± 0.01)	0.0043 (± 0.0001)
	O/N	3.4 (± 0.1)	1.99 (± 0.01)	0.0042 (± 0.0004)
1x(Zn+Pb) STEM	S	8. (± 0.1)	2.30 (± 0.01)	0.0000 (± 0.0013)
	O/N	3.5 (± 0.4)	1.99 (± 0.01)	0.0091 (± 0.0019)
5x(Zn+Pb) STEM	S	0.8 (± 0.6)	2.29 (± 0.01)	0.0107 (± 0.0116)
	O/N	3.4 (± 0.7)	2.06 (± 0.02)	0.0093 (± 0.0028)
5x(Zn+Pb) LEAF	S	2.1 (± 0.2)	2.29 (± 0.01)	0.0059 (± 0.0010)
	O/N	3.3 (± 0.7)	2.05 (± 0.02)	0.0168 (± 0.0041)
	C	1.1 (± 0.6)	3.01 (± 0.03)	0.0060 (± 0.0091)

The fit for 5x(Zn+Pb) leaf material produced different results from those derived for the stem and Bytom crop samples. The first shell coordination numbers were 2.1 (± 0.2) S, and 3.3 (± 0.7) O/N at distances 2.29 (± 0.01) Å and 2.05 (± 0.02) Å, respectively. The fit was improved through the inclusion of C in the second shell with a coordination number of 1.1 (± 0.6) at distance 3.01 (± 0.03) Å. Inclusion of C in the second shell was statistically justified by significantly lower reduced chi-square for improving the overall fit quality. This fit was markedly different from the others, as the sum of the coordination numbers for the first shell was 5.4 (± 0.7) suggesting a higher proportion of the Zn in an octahedral coordination environment.

The EXAFS fits show that the S bond distances were the same within error (2.27–2.30 Å) for all the samples presented in Table 6, and in good agreement with tetrahedrally coordinated Zn-S ligands reported for Zn-cysteine standards (Table 7). However, the differences in the O/N bond lengths for some of the samples were beyond the error of the fits. Both the Bytom field crop and stem material from the 1x(Zn+Pb) pot trial have O/N bond distance 1.99 (± 0.01) Å. Short radial distances for O/N were similar to those reported for Zn incorporation in cell wall materials, pectin or phosphates, or Zn-histidine with its tetrahedral N coordination. In contrast, both the stem and leaf materials from the 5x (Zn+Pb) pot trial returned radial distances for O/N of 2.05 (± 0.01) and 2.06 (± 0.01) Å, respectively. This longer bond distance was consistent with the presence of Zn-malate where Zn is octahedrally coordinated with O (Table 7).

4. Discussion

4.1. Uptake by pot trial plants

Miscanthus biomass from a long-term field-trial had elevated Zn and

Table 7
EXAFS fitting parameters reported for Zn compounds.

Sample	Path	CN	R (Å)	σ^2 (Å^2)
Zn-Histidine (solution)[1]	N	3.8	2.03	0.0067
	O	(± 0.2)	(± 0.02)	(± 0.0021)
	C	1.3	2.91	0.0092
		(± 0.4)	(± 0.02)	(± 0.0034)
		3.9	3.01	0.0051
		(± 0.6)	(± 0.03)	(± 0.0024)
Zn-Malate (solution)[1]	O	6.0	2.08	0.0101
	C	(± 0.2)	(± 0.02)	(± 0.0032)
		2.9	2.85	0.0056
		(± 0.5)	(± 0.03)	(± 0.0022)
Zn-Malate (solution)[2]	O	6.0	2.07	0.007
	C	(± 0.6)	(± 0.01)	0.010
		2.8	2.86	
		(± 0.6)	(± 0.02)	
Zn-Cell Wall[2]	O	4.6	2.00	0.010
	C	(± 0.5)	(± 0.01)	0.010
		1.3	2.83	
		(± 0.3)	(± 0.02)	
Zn-Pectin[2]	O	4.9	2.02	0.010
	C	(± 0.5)	(± 0.01)	0.010
		2.4	2.86	
		(± 0.5)	(± 0.02)	
Zn-Phosphate[2]	O	3.8	1.97	0.008
	P	(± 0.4)	(± 0.01)	0.010
		0.4	2.94	
		(± 0.8)	(± 0.02)	
Zn-Cysteine (solution)[1]	S	4.0 *	2.29	0.0081
			(± 0.02)	(± 0.0021)
ZnS[3]	S	3.8	2.34	NR
	Zn	NR	3.90	NR

References:
[1] (Mishra et al., 2020)
[2] (Sarret et al., 2009)
[3] (Valeev et al., 2011)
* set to crystallographic standard number

Pb concentrations relative to reported values for *Miscanthus* plants grown in uncontaminated soil, indicating that growth at a Zn and Pb contaminated site resulted in up-take of these metals. Similar uptake of Zn and Pb has been reported for other *Miscanthus* species (Wang et al., 2012; Wanat et al., 2013; Barbosa et al., 2015; Kocoń and Jurga, 2017). The uptake of Zn/Pb by the Bytom Crop was replicable in short-term pot-trials, which also showed a positive relationship between observed metal concentrations in both the stems and leaves, and the metal concentration in the soil.

The data for Zn uptake by stem and leaf sample from the pot trail were modelled using an exponential curve function (Fig. 5). The plots illustrate a non-linear relationship between Zn concentration in the soil and resultant biomass concentrations. In both the stem and leaf material, the initially rapid increase in uptake as the soil Zn concentration increases from low levels was followed by incrementally smaller increases at higher soil Zn concentrations. This plateauing was most visible in the stem material, where the highest Zn concentrations were observed, and suggests there may be a limit to the amount of Zn that can be taken-up by the biomass.

A positive correlation was also identified for the uptake of Pb from the soil in the pot trials. However, there was greater scatter in the data, particularly at lower soil Pb concentrations, which resulted in greater uncertainty in curve fitting (Fig. 6).

4.2. Zn and Pb distribution

A difference between Zn and Pb uptake was also observed in the spatial distribution of these PTEs between stem and leaf structures. The pot-trial data from this study showed that Zn accumulates to a greater extent in the stem structures than in the leaves, whereas the opposite was true for Pb. Across the 1x(Zn+Pb) replicates the median values for Zn were 400 and 109 mg/kgdm for stem and leaf respectively, and 1 and 4 mg/kgdm for Pb. These observed differences in distribution between stem and leaf were statistically significant for both Zn (Mann-Whitney U $= 0$, $n_1 = n_2 = 5$, $p < 0.05$ two-tailed) and Pb (Mann-Whitney U $= 24.5$, $n_1 = n_2 = 5$, $p < 0.05$ two-tailed). The data for seed-based hybrid used in this study conformed with the pattern observable in data from previous studies for both Zn and Pb in *Miscanthus x giganteus* hybrid (Wanat et al., 2013; Andrejić et al., 2018).

4.3. Pot trial plants vs mature crop

In the long-term Bytom field trial, mature *Miscanthus* biomass was harvested following the winter senescence period in March 2018. This is normal time of year for harvesting *Miscanthus* crops. This biomass consisted predominantly of stem material, and it contained an elevated Zn concentration (94 mg/kg$_{(dm)}$) relative to reported values *Miscanthus* plants grown in uncontaminated soil. However, this Zn loading was lower than that observed with actively growing juvenile plants in the pot trials containing similar levels of bioavailable Zn (where the stem biomass contained 387 mg/kg$_{(dm)}$ while the leaf biomass contained 111 mg/kg$_{(dm)}$). Rusinowski et al. (2019a) analysed Zn uptake by the same hybrid grown at Bytom at the end of its second growing season in September/October 2016 and reported that the Zn concentration within the 'shoots' was 213.1 mg/kg$_{(dm)}$. While Rusinowski's data were not disaggregated into different plant structures, the value is midway between the values for the 'stem' and 'leaf' material for the 1x(Zn+Pb) plants in this study, and higher than that determined for the mature biomass at time when the crop was harvested.

In the juvenile plants under 1x (Zn+Pb) soil conditions, the Pb concentration was lower in all structures (stem 1.4 mg/kg$_{(dm)}$ and leaf 3.6 mg/kg$_{(dm)}$) than that observed in the biomass from the Bytom field

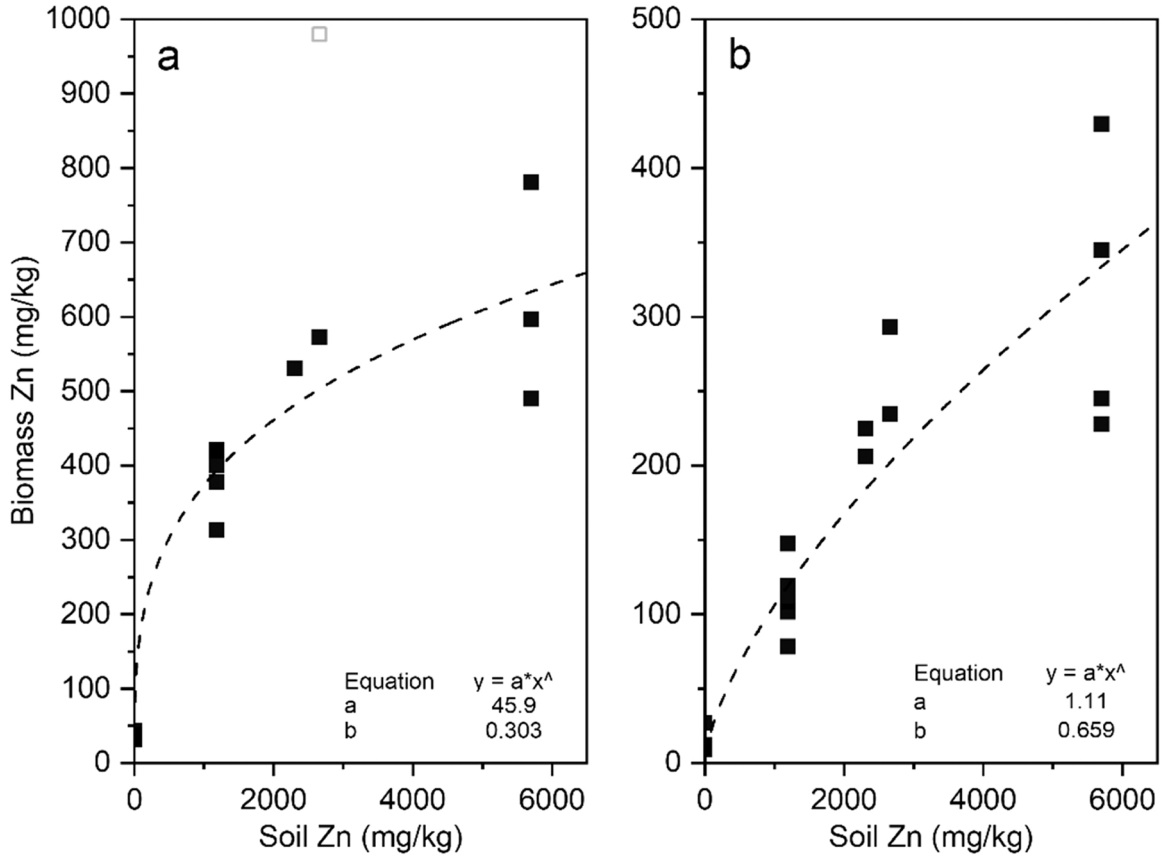

Fig. 5. exponential curve fits for Zn uptake in (a) stem and (b) leaf structures of growth trial plants. Soil Zn concentration are reported as sum of the bioavailable fractions (chloride and carbonate). Single outlier point (980 mg/kg) in the stem data is masked during the fitting process.

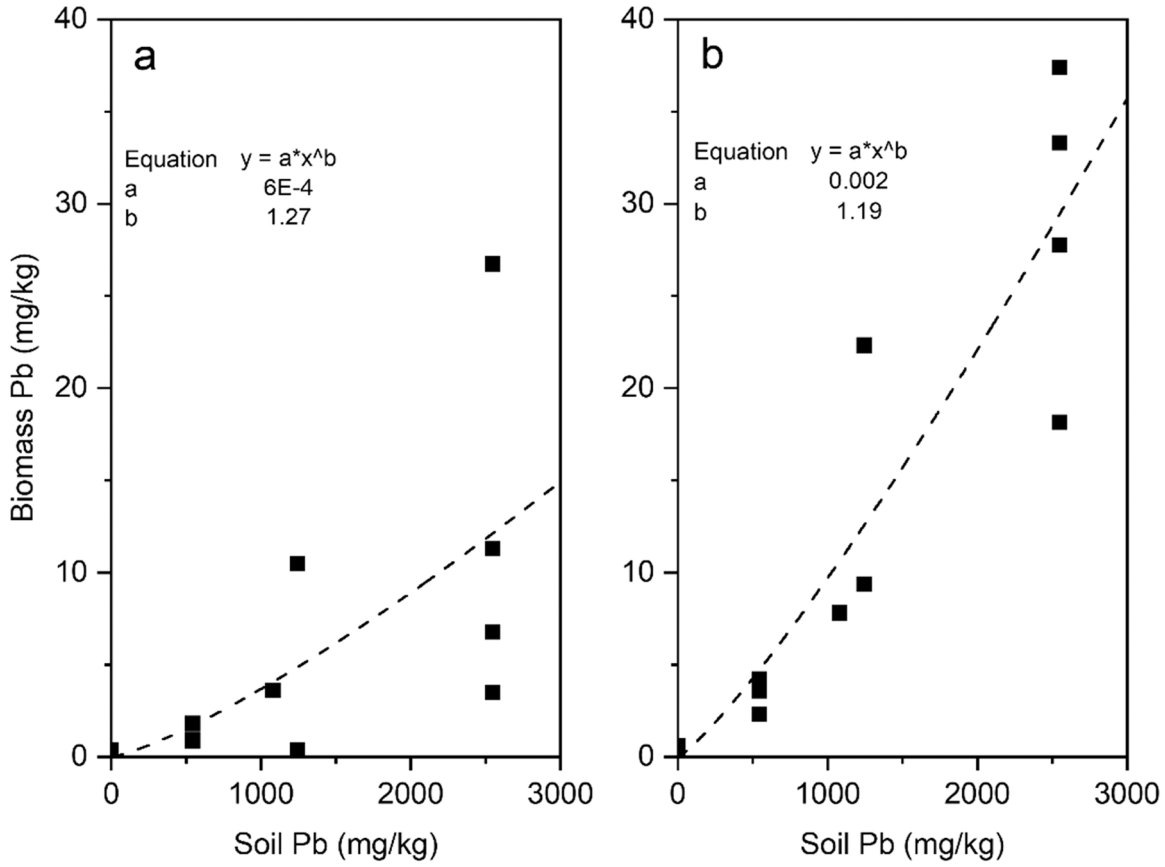

Fig. 6. exponential curve fits for Pb uptake in (a) stem and (b) leaf structures of growth trial plants. Soil Pb concentration are reported as sum of the bioavailable fractions (chloride and carbonate).

trial (14.4 mg/kg$_{(dm)}$). Rusinowski et al. (2019a) report Pb values of 22.2 ± 2.27 mg/kg$_{(dm)}$ for the same hybrid grown at the Bytom site at the end of the 2016 growing period. Hence, the data suggest that Pb uptake increases over the long-term with the lowest values being observed in the juvenile plants indicating a fundamentally different uptake mechanism. Nonetheless, Pb concentrations measured in this study after winter senescence was lower than the value measured during the 2016 growing season by Rusinowski et al. (2019a). The data suggest that the uptake and/or sequestration mechanism for Pb was different from Zn.

Senescence of *Miscanthus* has been demonstrated to produce significant changes in the biomass concentration of major cations and anions: K, P, Cl and S are known to decrease over the winter period, Si and Na increase while Ca is little affected (Baxter et al., 2012). However, the effect of senescence on trace metals such as PTEs is so far not well documented in literature. The combination of this study and data from Rusinowski et al. (2019a) indicates that winter senescence may result in a reduction of biomass Zn concentration compared with that observed during growth phases. This would be consistent with two studies conducted by Rusinowski on *Miscanthus x giganteus* grown at the Bytom site, which show a reduction in biomass Zn concertation between September 2016 and March 2017 (Rusinowski et al., 2019a; Rusinowski et al., 2019b). These data do not conform with observations made by Krzyzak et al. (2017) which reports that winter senescence resulted in no significant change or even increase in Zn within aerial structures of *Miscanthus x giganteus* and other *Miscanthus* hybrids. Krzyzak et al. do, however, concluded that Zn uptake/sequestration was species-specific with different behaviours being observed between species. The lower abundance of Zn may therefore be specific to the specific hybrid used here.

4.4. Zn speciation

Zinc is an essential plant micronutrient required as a constituent of several enzymes and proteins (Broadley et al., 2007; Sharma et al., 2013). However, relatively small quantities of Zn in soil are sufficient (~20 mg/kg$_{(dm)}$; (Suganya et al., 2020)) and the normal range for Zn in plant tissue is 15–60 mg/kg $_{(dm)}$ (Singh, 1986; Venkatesh et al., 2014). Excess Zn is toxic, so plants can adopt different mechanisms to sequester surplus Zn within their cells. These mechanisms include: complexation within the cytosol with organic acids or metal-binding peptides, compartmentalisation within cell walls, and compartmentalisation within the cell vacuole (Hall, 2002; Broadley et al., 2007). Plants contain a range of organic molecules that can act as ligands to Zn, including organic acids (e.g. citrate, malate, oxalate), phytate (a hexa-phosphate that is the main storage form of phosphorus in the seeds), amino acids (e.g. histidine and cysteine), metallothioneins (MTs; cysteine-rich proteins), and phytochelatins (PC, oligomers of glutathione, a tripeptide of glutamate, cysteine and glycine) (Mathys, 1977; Ernst et al., 1992; Verkleij et al., 1998; Sarret et al., 2002; Mishra et al., 2020).

The XANES LCF approach included four Zn-complexes; Zn-malate, Zn-histidine, Zn-cysteine and ZnS. Each spectrum was included in the LCF analysis through a combinatorial approach - sequentially adding one of the remaining spectra to the previous best fit and its inclusion was justified by a significant lowering of the reduced chi-square value. The LCF methodology was consistent in selecting ZnS as being present alongside Zn-cysteine. The precipitation of nanoscale sulfide crystals has been reported in plants grown under PTE stress, in particular with regards to Cd contamination (Dameron et al., 1989; Reese et al., 1992; Neumann and Zur Nieden, 2001; Carrier et al., 2003). The potential presence of sulfide crystals in the *Miscanthus* samples was therefore considered.

ZnS crystals can be unambiguously identified using EXAFS due to strong scattering paths arising from Zn in the second coordination shell: nano-scale ZnS exhibits tetrahedral coordination with S in the first shell of 2.34 Å and a second shell comprised of Zn at 3.90 Å (Valeev et al., 2011). The scattering paths associated with the presence Zn in the second shell are clearly distinguished via a peak at ~3.90 Å in the magnitude of the FT of the ZnS standard (Fig. 4a). None of the EXAFS FTs for the samples exhibit this characteristic peak (Fig. 4c) so the presence of ZnS nanocrystals can be ruled out on this basis. Nonetheless, the LCFs strongly suggested the need for a contribution from signal at a lower energy regime (E_0 ~9662 eV), around the peak position for ZnS which is lower than Zn-cysteine peak position. The XANES spectrum for the aqueous Zn-cysteine might not serve as the best standard for higher molecular weight (cysteine rich) complexes, such as Zn-PC and Zn-MT due to differences in local S coordination environment. These differences may, at least in part, be compensated for by the features of the ZnS spectrum. The pathways for PTE sequestration involving S are complex at the intracellular level, e.g. detoxification of Cd includes low molecular weight PCs in the cytosol acting as a shuttle to the vacuole, wherein Cd sequestration is achieved by the incorporation with S^{2-} in high molecular weight complexes (Clemens, 2001; Cobbett and Goldsbrough, 2002). The presence of S^{2-} within a PC complex results in higher metal binding capacity and improved effectiveness of PTE sequestration (Steffens, 1990). The LCF results in this study pointed towards Zn-cysteine alone as being an imperfect representation of a more complex S ligation environment within *Miscanthus*.

A further pattern of S ligation was evident within the LCF data. The S signal (Fig. 3; combined contributions of Zn-cysteine and ZnS) was more prevalent in the leaf material than the stem materials, which in turn were greater than the Bytom crop (Table 6). The more detailed assessment of Zn coordination environments using EXAFS fitting confirms the same general pattern for the prevalence of S ligands, i.e. pot trial leaf > pot trial stem > Bytom crop. First shell coordination numbers for S range from the highest of 2.1 (± 0.02) in the leaf, to 0.8 (± 0.6) in both stem samples, and 0.7 (± 0.1) in the Bytom crop. The coordination number of S for stem and the Bytom sample (which was mostly stem) was similar within error. The coordination number for S in the leaf sample was substantially higher which indicates that the biochemistry for Zn within the leaf was different. The EXAFS fit result for the leaf sample suggested that S ligands comprise around half of the Zn coordination environment in the leaf, compared to only around a fifth of that in stem samples. The EXAFS data should be viewed in conjunction with the data for bulk Zn concentration within the samples (Fig. 1), which together show that higher S ligation in the leaf was associated with a comparatively low Zn concentration. The stem samples had a higher Zn concentration but with the EXAFS fitting suggesting lower prevalence of S ligands (Fig. 7). It is entirely possible that -SH ligands are higher affinity yet lower abundance binding sites providing an important complexation mechanism for Zn in stem but were masked by higher abundance of O/N sites.

The EXAFS fitting data for O/N species provide further insight into the pattern of Zn complexes within *Miscanthus*. It is not possible to directly differentiate between O and N species using EXAFS due to similar atomic numbers giving a similar scattering signal. However, the coordination geometry (bond length and coordination number) of the fits can provide information about the likely Zn ligands present in the samples. In Zn-organic acid complexes, the Zn tends to be octahedrally coordinated with O-ligands, with a typical bond length 2.07–2.08 Å (Sarret et al., 2009; Mishra et al., 2020). In Zn-phytate complex, Zn is tetrahedrally coordinated with O-ligands, with a bond length of 1.96 Å (Sarret et al., 2002). With amino acids, Zn can coordinate with elements in sidechains, and thus the coordination environment varies with the type of amino acid. Zn-histidine has been adopted as a standard to represent amino acid complexes; here Zn is tetrahedrally coordinated with N with typical bond lengths of 2.03 Å (Thomas et al., 2019; Mishra et al., 2020).

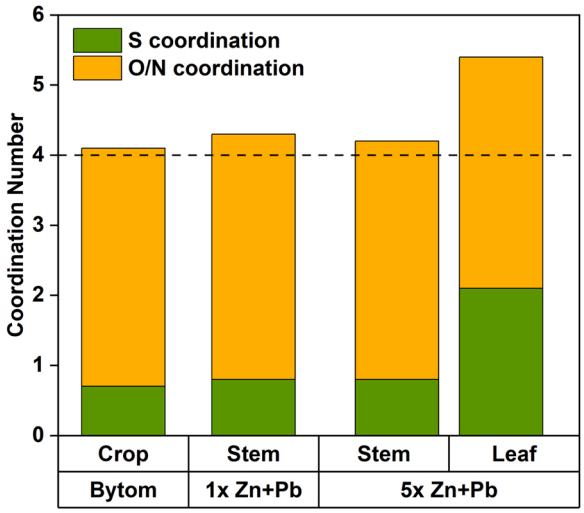

Fig. 7. coordination numbers derived from EXAFS fitting of samples.

The individual O/N coordination numbers across all samples were remarkably similar (3.3 – 3.5) within error (Table 6). However, O/N coordination numbers does not provide the full picture unless viewed in conjunction with the S coordination numbers for the first shell. The total coordination number for the leaf sample has a higher value of 5.4 (± 0.7), followed by stem samples from the pot trials 4.3 (± 0.3) - 4.2 (± 0.7) with the 5x(Zn+Pb) sample having the larger uncertainty; and the Bytom crop has the lowest value of 4.1 and the smallest uncertainty. The high value (CN → 6) for the leaf sample was consistent with octahedral O/N being present and therefore that Zn-O/N ligands being associated with organic acid complexes. A presence of organic acid complexes in the leaf was supported by the fit of bond length being 2.05 (± 0.02) Å which is near the upper end of the range associated with tetrahedral O/N bond lengths and is associated with octahedral O/N geometry, as represented by Zn-malate (2.07–8 Å; Table 7).

The data for O/N bond lengths across the stem samples display a range of values from 2.06 to 1.99 Å. The 5x(Zn+Pb) stem samples was best fit with a longer bond length of 2.06 (± 0.02) Å, suggesting the predominance of Zn complexation by organic acids. The data for the Bytom crop sample was most closely aligned with O/N being in a tetrahedral form as the bond distance was best fitted at 1.99 (± 0.01) Å. The 1x(Zn+Pb) stem had a similar fit to the Bytom crop with a result of 1.99 (± 0.01) Å also indicating a tetrahedral coordinated O/N environment but within a more disordered system (higher σ^2) which suggests greater uncertainty/heterogeneity. The variations in the bond length data as well as Zn coordination environment suggests a continuum in the Zn speciation facilitated by the O/N ligand in stem materials – with octahedral/organic acid species most prevalent in the samples with the highest Zn concentration, whereas tetrahedral species were more prevalent at lower Zn concentration, especially in the mature crop. This suggests that Zn has a higher initial affinity for tetrahedral coordination geometry at lower Zn concentrations, with octahedral geometry becoming increasingly apparent only as Zn concentration increases.

The lowest O/N bond lengths in the samples, found in the Bytom crop, were closely comparable to those reported by Sarret et al. (2009) (Table 7) for incorporation of Zn within cell wall and pectin (a proxy for cell walls) material. Spatially resolved data of cellular structures would be required to confirm Zn sequestration within cell walls. Furthermore, as EXAFS data represent the averaged signal for Zn speciation throughout the entire sample, combinations of species including, for example, Zn-phosphate which has the shortest bond length (1.97 (± 0.01) Å; Table 7) mixed with other species such as Zn-histidine cannot be ruled out by the bulk analyses presented in this work.

4.5. Limitations of XAFS techniques

The bulk XAFS analyses presented in this study are constrained by the loss of spatially resolved information. Due to the homogenisation of samples, there is a complete loss of spatial information regarding potential variation in PTE storage across different tissue structures (e.g. epidermis vs vascular tissues). However, some ligands have been shown in previous research to be associated with specific sub-cellular organelles. Identification of such ligands within the bulk samples could therefore provide insights into PTE distribution on a cellular level - this is discussed below.

The LCF results for Zn identified tetrahedral O/N coordination in the samples. There are a range of possible tetrahedral species, including pectin and histidine ligands, which occur throughout cell structures. Therefore, the LCF data by themselves provide no information regarding spatial distribution. The data from the EXAFS fitting, however, indicate that O/N bond length in the Bytom crop and 1x(Zn+Pb) Stem samples is at the lower end of the range for tetrahedral O/N coordination. The shorter bond length is indicative of pectin/cell wall ligands, rather than the Zn-histidine standard solution. There is, therefore, evidence in the EXAFS data that these samples have significant Zn sequestration within the cell wall compartment. All other samples demonstrated longer O/N bond lengths indicating either Zn-histidine, or increasing amounts of octahedral species such as organic acids (e.g. Zn-malate), which suggests Zn as being complexed somewhere within the cytoplasm rather than the cell wall. However, no conclusions can be made regarding the location of Zn complexation within the cytoplasm.

S ligands, such as PT and MT, have been implicated with vacuolar sequestration and may act as a shuttle mechanisms to transfer PTEs from the cytosol into the vacuole (Clemens, 2001, Cobbett et al., 2002). XANES LCF results identified a greater predominance of S species within the leaf samples. However, EXAFS FT analysis did not suggest sulfide nanocrystals in any sample, which could have been an indicator of sequestration within vacuoles (Dameron et al., 1989; Reese et al., 1992; Neumann and Zur Nieden, 2001; Carrier et al., 2003). The XAFS data for S is therefore non-specific with respect to spatial distribution, other than indicating Zn is present in the cytoplasm and not suggestive of incorporation within the cell wall, where O/N bonding is expected.

The limit of spatial information within the XAFS data is suggestive of compartmentalisation within the cell wall being more prevalent in the Bytom crop, and to a lesser extent the 1x(Zn+Pb) stem, compared with other samples. Although the predominance of S species in the leaves compared to stem suggest differences in Zn sequestration mechanism within the cytoplasm, it is insufficient to identify the organelles involved in sequestration of Zn. Spatially resolved elemental mapping through application of techniques such as μXRF microscopy would be required to provide any spatial conclusions.

As is true for any technique, XAFS studies of elemental speciation in biological samples have their own challenges. Challenges may arise through the potential for artifacts occurring in the data as a result of sample preparation or X-ray induced chemical change. For example, sample preparation through dehydration could potentially result in water-bound complexes being replaced by other ligands. Similarly, use of formaldehyde for fixing biological tissues has been shown to introduce artifacts into XAFS results (Lombi et al., 2011; Porcaro et al., 2018). The X-ray beam could result in mass loss due to heat generation and chemical changes may occur either directly as a result of photo-induced redox transformations or indirectly via the formation of highly reactive free radicals within the samples (Weik et al., 2000).

Sample preparation impacts are known to occur on elements with redox sensitive chemistry (e.g., S and Hg). Consequently, XAFS measurement of redox sensitive samples is recommended under cryogenic conditions (Hackett et al., 2012). However, in-vivo studies of more stable elements in plants, such as Fe(III), suggest drying does not significantly impact XAFS results and adopting less intensive sample preparation protocols may be preferable (Bacquart et al., 2007). Furthermore, removal of water helps minimise X-ray induced free radical formation, with both freeze-drying and air drying delivering comparable results (Hackett et al., 2012). In experiments similar to this study, Isaure et al. used XANES to examine speciation of Cd speciation in plant (*Arabidopsis thaliana*) samples, comparing the results from freeze-dried samples measured at ambient temperature with hydrated samples under cryogenic conditions. No significant difference between the two samples was observed and it was concluded that Cd speciation is not noticeably altered by freeze-drying. Indeed, the hydrated cryogenic sample produced noisier spectra as a result of the lower Cd concentration and greater absorption of the fluorescence (Isaure et al., 2006). Therefore, the drying of samples appears appropriate when studying redox stable species (e.g., Zn) in plant samples.

The extent to which beam damage may impact results depends on the precise nature of the sample. Some organic acid-metal complexes such as malate are stable, whilst others such as nicotianamide have been found to be unstable, even under cryogenic conditions (Terzano et al., 2013). Similarly, many cysteine and histidine bonds are considered relatively stable for synchrotron experiments barring a few specific exceptions (Weik et al., 2000). Evidence of X-ray beam induced changes can be monitored by comparing XANES spectra of sequential scans (Bacquart et al., 2007). If multiple scans are recorded and subsequently compared with each other, beam damage reveals itself through changes in the spectra across the sequence. Changes in the white line feature of the XANES spectra suggest alteration of the coordination environment, and any shift in energy peak position suggests a change in the redox state of the element under probe. Under the environmental conditions used for this study, Zn is highly redox stable and evidence of progressive changes in spectra which could signify beam damage were not observed (see SI Figure S5 for comparison of sequential scans).

Nonetheless, it is important to note that XAFS can only provide insights into the speciation of the element under probe (e.g., Zn). A complementary line of research may be measuring expression (either up or down regulation) of organic acids in plant tissues due to the presence of contaminants. Techniques such as chromatography may be more appropriate for such analysis, but has its own issues of interpretation and sample preparation and is out of scope of this study.

5. Conclusions

The uptake of Zn and Pb by a novel seed-based hybrid of *Miscanthus* has been studied in detail. Positive correlations between concentrations of bioavailable Zn and Pb in the soil and subsequent uptake by the plants has been demonstrated in juvenile plants. Uptake by juvenile plants has been shown to contain higher concentrations of Zn but lower concentrations of Pb than that reported for mature plants grown in similar soil conditions. Statistically significant differences between metals' concentrations in the stem and leaf materials have been demonstrated, with opposing patterns for Zn and Pb suggesting that different uptake mechanisms were at play. The XAFS analyses of Zn has shown that unique patterns of speciation exist in different plant structures. Leaves were associated with higher prevalence of S ligands compared with that observed in stem material and mature crop material. Leaves were also associated with a high coordination number for O/N suggesting organic acid ligands play a large role in Zn ligation within the leaf. Stem structures had a lower O/N coordination number associated with shorter bond lengths, which is consistent with tetrahedral species of histidine-like amino acids or a pectin/cell wall coordination environment. The mature (post-senescence) crop material had a distinct spectrum with the lowest prevalence of S species and a high prevalence of tetrahedral O/N species at radial distances consistent Zn complexation within a pectin/cell wall environment.

Environmental implication

Heavy Metal (HM) contaminated soils present long-term hazards to

human-health and the environment. Understanding the fate of HM in plants grown on contaminated lands is key to evaluating potential land use for cultivating non-edible crops such as biofuels. This work presents systematic studies for the uptake, distribution, and sequestration of Zn and Pb by a novel Miscanthus hybrid grown in contaminated soils. HM concentrations are quantified across aerial biomass structures in response to varying levels of soil contamination. Contaminant distribution and sequestration mechanisms employed by Miscanthus will help determine its biofuel value without competing with food crops.

CRediT authorship contribution statement

Innes Deans: Conceptualization, Investigation, Formal analysis, Writing – original draft, Visualization. **Douglas I. Stewart:** Methodology, Writing – review & editing. **Jenny Jones:** Funding acquisition. **Jason Kam:** Resources. **Bhoopesh Mishra:** Conceptualization, Funding acquisition, Methodology, Investigation, Writing – review & editing, Validation, Supervision.

Declaration of Competing Interest

The authors declare that they have no known competing financial interests or personal relationships that could have appeared to influence the work reported in this paper.

Data Availability

Data will be made available on request.

Acknowledgements

The authors acknowledge the support of: Terravesta Ltd. (UK) for their support in provision of the *Miscanthus* plants; Bell Brothers Nursery Ltd (UK) for seed germination through and initial cultivation of *Miscanthus* plants; the staff at Spen Farm (University of Leeds) (UK) for facilitating collection of soil; Simon Lloyd (University of Leeds) for running the ICP-MS analyses; and Stella Foster for help with collection of XAFS data. XAFS data was collected at MRCAT (beamline 10-BM-B) of the Advanced Photon Source, Argonne National Laboratory. MRCAT operations are supported by the Department of Energy and the MRCAT member institutions. This research used resources of the Advanced Photon Source, a U.S. Department of Energy (DOE) Office of Science User Facility operated for the DOE Office of Science by Argonne National Laboratory under Contract No. DE-AC02–06CH11357. Innes Deans was funded through EPSRC CDT in Bioenergy (grant reference: EP/L014912/1) for this study. *Miscanthus* seed-based hybrid cultivar used in this project were developed with support from the UK's Biotechnology and Biological Sciences Research Council (BBSRC) and Department for Environment, Food and Rural Affairs (DEFRA) through the GIANT-LINK project (LK0863) and by the Innovate UK/BBSRC 'MUST' BB/N016149/1 project. We also thank Dick Flavell and Ceres for the uses of the *Miscanthus* cultivars, which were bred at Aberystwyth University, IBERS, under the leadership of John Clifton-Brown, the research group leader for Plant Biology for the Sustainable Bio-economy. The authors would like to thank the Institute for Ecology of Industrial Areas, Katowice, Poland, for providing soil and plant samples from the Miscanthus field experiment, operated under MISCOMAR + project. This project is funded by The Polish National Centre for Research and Development, under the flag of Era-Net Cofound FACCE SURPLUS, in the frame of the Joint Programming Initiative on Agriculture, Food Security and Climate Change (FACCE-JPI), grant number FACCE SURPLUS/III/MISCOMAR+/03/2020.

Appendix A. Supporting information

Supplementary data associated with this article can be found in the online version at doi:10.1016/j.jhazmat.2022.129899.

References

Adediran, G.A., Ngwenya, B.T., Mosselmans, J.F., Heal, K.V., Harvie, B.A., 2015. Mechanisms behind bacteria induced plant growth promotion and Zn accumulation in Brassica juncea. J. Hazard. Mater. 283, 490–499.

Adediran, G.A., Ngwenya, B.T., Mosselmans, J.F., Heal, K.V., Harvie, B.A., 2016a. Mixed planting with a leguminous plant outperforms bacteria in promoting growth of a metal remediating plant through histidine synthesis. Int. J. Phytoremediat. 18, 720–729.

Adediran, G.A., Ngwenya, B.T., Mosselmans, J.F.W., Heal, K.V., 2016b. Bacteria-zinc co-localization implicates enhanced synthesis of cysteine-rich peptides in zinc detoxification when Brassica juncea is inoculated with Rhizobium leguminosarum. New Phytol. 209, 280–293.

Adele, N.C., Ngwenya, B.T., Heal, K.V., Mosselmans, J.F.W., 2018a. Soil bacteria override speciation effects on zinc phytotoxicity in zinc-contaminated soils. Environ. Sci. Technol. 52, 3412–3421.

Adele, N.C., Ngwenya, B.T., Heal, K.V., Mosselmans, J.F.W., 2018b. Soil bacteria override speciation effects on zinc phytotoxicity in zinc-contaminated soils. Environ. Sci. Technol. 52, 3412–3421.

Al Souki, K.S., Liné, C., Moravec, J., Douay, F., Pourrut, B., 2022. Response of three miscanthus x giganteus cultivars to toxic elements stress: part 2, comparison between two growing seasons. Plants 11 (7).

Andrejić, G., Gajić, G., Prica, M., Dželetović, Ž., Rakić, T., 2018. Zinc accumulation, photosynthetic gas exchange, and chlorophyll a fluorescence in Zn-stressed Miscanthus × giganteus plants. Photosynthetica 1–10.

Angelova, V., Zapryanova, V., 2021. Miscanthus x giganteus as a biofuel crop for phytoremediation of heavy metal contaminated soils. Sci. Papers. Ser. E Land Reclam Earth Obs. Surv. Environ. Eng. 10, 192–203.

Bacquart, T., Devès, G., Carmona, A., Tucoulou, R., Bohic, S., Ortega, R., 2007. Subcellular speciation analysis of trace element oxidation states using synchrotron radiation Micro-X-ray absorption near-edge structure. Anal. Chem. 79 (19), 7353–7359.

Barbosa, B., Boléo, S., Sidella, S., Costa, J., Duarte, M.P., Mendes, B., Cosentino, S.L., Fernando, A.L., 2015. Phytoremediation of heavy metal-contaminated soils using the perennial energy crops Miscanthus spp. and Arundo donax L. Bioenergy Res. 8, 1500–1511.

Baxter, X.C., Darvell, L.I., Jones, J.M., Barraclough, T., Yates, N.E., Shield, I., 2012. Study of Miscanthus x giganteus ash composition - variation with agronomy and assessment method. Fuel 95, 50–62.

Baxter, X.C., Darvell, L.I., Jones, J.M., Barraclough, T., Yates, N.E., Shield, I., 2014. Miscanthus combustion properties and variations with Miscanthus agronomy. Fuel 117, 851–869.

Broadley, M.R., White, P.J., Hammond, J.P., Zelko, I., Lux, A., 2007. Zinc in plants. New Phytol. 173, 677–702.

BSI, 2020. BS EN ISO 17225-7. Solid Biofuels. Fuel specifications and classes: Part 7. Graded non-woody briquettes. British Standards Institution.

Cadoux, S., Riche, A.B., Yates, N.E., Machet, J.M., 2012. Nutrient requirements of Miscanthus x giganteus: conclusions from a review of published studies. Biomass-.-. Bioenergy 38, 14–22.

Carrier, P., Baryla, A., Havaux, M., 2003. Cadmium distribution and microlocalization in oilseed rape (Brassica napus) after long-term growth on cadmium-contaminated soil. Planta 216, 939–950.

Castorina, E., Ingall, E.D., Morton, P.L., Tavakoli, D.A., Lai, B., 2019. Zinc K-edge XANES spectroscopy of mineral and organic standards. J. Synchrotron Radiat. 26, 1302–1309.

Cen 2014. ISO 17225–7 - Solid biofuels - Fuel specifications and classes Part 7: Graded non-woody briquettes.

Clemens, S., 2001. Molecular mechanisms of plant metal tolerance and homeostasis. Planta 212, 475–486.

Cobbett, C., Goldsbrough, P., 2002. Phytochelatins and metallothioneins: roles in heavy metal detoxification and homeostasis. Annu. Rev. Plant Biol. 53, 159–182.

Dameron, C.T., Reese, R.N., Mehra, R.K., Kortan, A.R., Carroll, P.J., Steigerwald, M.L., Brus, L.E., Winge, D.R., 1989. Biosynthesis of cadmium sulphide quantum semiconductor crystallites. Nature 338, 596–597.

Deng, H., Ye, Z.H., Wong, M.H., 2004. Accumulation of lead, zinc, copper and cadmium by 12 wetland plant species thriving in metal-contaminated sites in China. Environ. Pollut. 132, 29–40.

Ecn, 2018. *Phyllis2, database for biomass and waste* [Online]. Energy Research Centre of the Netherlands (Available). ⟨https://phyllis.nl/⟩.

Ernst, W.H.O., Verkleij, J.A.C., Schat, H., 1992. Metal tolerance in plants. Acta Bot. Neerl. 41, 229–248.

Esau, K. 1977. Anatomy of seed plants-2.

Evans, S.G., Ramage, B.S., Dirocco, T.L., Potts, M.D., 2015. Greenhouse gas mitigation on marginal land: a quantitative review of the relative benefits of forest recovery versus biofuel production. Environ. Sci. Technol. 49, 2503–2511.

Greef, J.M., Deuter, M., Hodkinson, T.R., Renvoize, S.A., 2001. Miscanthus x giganteus. Kew Bull. 56 (3), 759.

Hackett, M.J., Smith, S.E., Paterson, P.G., Nichol, H., Pickering, I.J., George, G.N., 2012. X-ray absorption spectroscopy at the sulfur K-edge: a new tool to investigate the biochemical mechanisms of neurodegeneration. ACS Chem. Neurosci. 3 (3), 178–185.

Hall, J.L., 2002. Cellular mechanisms for heavy metal detoxification and tolerance. J. Exp. Bot. 53, 1–11.

Isaure, M.-P., Fayard, B., Sarret, G., Pairis, S., Bourguignon, J., 2006. Localization and chemical forms of cadmium in plant samples by combining analytical electron microscopy and X-ray spectromicroscopy. Spectrochim. Acta Part B At. Spectrosc. 61 (12), 1242–1252.

Kelly, R.A., Andrews, J.C., Dewitt, J.G., 2002. An X-ray absorption spectroscopic investigation of the nature of the zinc complex accumulated in Datura innoxia plant tissue culture. Microchem. J. 71, 231–245.

Kisi, E.H., Elcombe, M.M., 1989. u parameters for the wurtzite structure of ZnS and ZnO using powder neutron diffraction. Acta Crystallogr. Sect. C: Cryst. Struct. Commun. 45, 1867–1870.

Kocoń, A., Jurga, B., 2017. The evaluation of growth and phytoextraction potential of Miscanthus x giganteus and Sida hermaphrodita on soil contaminated simultaneously with Cd, Cu, Ni, Pb, and Zn. Environ. Sci. Pollut. Res. 24, 4990–5000.

Korzeniowska, J., Stanislawska-Glubiak, E., 2015. Phytoremediation potential of Miscanthus × giganteus and Spartina pectinata in soil contaminated with heavy metals. Environ. Sci. Pollut. Res. 22, 11648–11657.

Krzyzak, J., Pogrzeba, M., Rusinowski, S., Clifton-Brown, J., Mccalmont, J.P., Kiesel, A., Mangold, A., Mos, M., 2017. Heavy metal uptake by novel miscanthus seed-based hybrids cultivated in heavy metal contaminated soil. Civ. Environ. Eng. Rep. 26, 121–132.

Kupper, H., Mijovilovich, A., Meyer-Klaucke, W., Kroneck, P.M.H., 2004. Tissue-and age-dependent differences in the complexation of cadmium and zinc in the cadmium/zinc hyperaccumulator Thlaspi caerulescens (Ganges ecotype) revealed by X-ray absorption spectroscopy. Plant Physiol. 134, 748–757.

Lewandowski, I., Heinz, A., 2003. Delayed harvest of miscanthus—influences on biomass quantity and quality and environmental impacts of energy production. Eur. J. Agron. 19, 45–63.

Li, C., Xiao, B., Wang, Q.H., Yao, S.H., Wu, J.Y., 2014. Phytoremediation of Zn- and Cr-contaminated soil using two promising energy grasses. Water, Air, Soil Pollut. 225.

Li, Y., Wang, Y., Zhang, Q., Hu, W., Zhao, J., Chen, Y., Zhong, H., Wang, G., Zhang, Z., Gao, Y., 2019. Elemental sulfur amendment enhance methylmercury accumulation in rice (Oryza sativa L.) grown in Hg mining polluted soil. J. Hazard. Mater. 379, 120701.

Lombi, E., Susini, J., 2009. Synchrotron-based techniques for plant and soil science: opportunities, challenges and future perspectives. Plant Soil 320, 1–35.

Lombi, E., Scheckel, K.G., Kempson, I.M., 2011. In situ analysis of metal(loid)s in plants: state of the art and artefacts. Environ. Exp. Bot. 72 (1), 3–17.

Luo, L., Shen, Y., Wang, X., Chu, B., Xu, T., Liu, Y., Zeng, Y., Liu, J., 2018. Phytoavailability, bioaccumulation, and human health risks of metal(loid) elements in an agroecosystem near a lead-zinc mine. Environ. Sci. Pollut. Res. 25 (24), 24111–24124.

Mathys, W., 1977. The role of malate, oxalate, and mustard oil glucosides in the evolution of zinc-resistance in herbage plants. Physiol. Plant. 40, 130–136.

Medas, D., De Giudici, G., Pusceddu, C., Casu, M.A., Birarda, G., Vaccari, L., Gianoncelli, A., Meneghini, C., 2019. 'Impact of Zn excess on biomineralization processes in Juncus acutus grown in mine polluted sites'. J. Hazard. Mater. 370, 98–107.

Mishra, B., Boyanov, M., Bunker, B.A., Kelly, S.D., Kemner, K.M., Fein, J.B., 2010. High- and low-affinity binding sites for Cd on the bacterial cell walls of Bacillus subtilis and Shewanella oneidensis. Geochim. Et. Cosmochim. Acta 74, 4219–4233.

Mishra, B., Mcdonald, L., Roy, M., Lanzirotti, A., Myneni, S., 2020. Uptake and speciation of zinc in edible plants grown in smelter contaminated soils. PLoS One 15 (4).

Neal, A.L., Geraki, K., Borg, S., Quinn, P., Mosselmans, J.F., Brinch-Pedersen, H., Shewry, P.R., 2013. Iron and zinc complexation in wild-type and ferritin-expressing wheat grain: implications for mineral transport into developing grain. JBIC J. Biol. Inorg. Chem. 18, 557–570.

Neumann, D., Zur Nieden, U. 2001. Silicon and heavy metal tolerance of higher plants. Phytochemistry, 56, 685–92 NOAA 2008.Screening Quick Reference Tables. NRM 2017. Analytical Report.

Nsanganwimana, F., Al Souki, K.S., Waterlot, C., Douay, F., Pelfrêne, A., Ridošková, A., Louvel, B., Pourrut, B., 2021. Potentials of Miscanthus x giganteus for phytostabilization of trace element-contaminated soils: ex situ experiment. Ecotoxicol. Environ. Saf. 214, 112125.

Pidlisnyuk, V., Erickson, L., Stefanovska, T., Popelka, J., Hettiarachchi, G., Davis, L., Trogl, J., 2019. Potential phytomanagement of military polluted sites and biomass production using biofuel crop miscanthus x giganteus. Environ. Pollut. 249, 330–337.

Porcaro, F., Roudeau, S., Carmona, A., Ortega, R., 2018. Advances in element speciation analysis of biomedical samples using synchrotron-based techniques. TrAC Trends Anal. Chem. 104, 22–41.

Pushie, M.J., Pickering, I.J., Korbas, M., Hackett, M.J., George, G.N., 2014. Elemental and chemically specific X-ray fluorescence imaging of biological systems. Chem. Rev. 114, 8499–8541.

Qin, Z., Zhuang, Q., Zhu, X., Cai, X., Zhang, X., 2011. Carbon consequences and agricultural implications of growing biofuel crops on marginal agricultural lands in China. Environ. Sci. Technol. 45, 10765–10772.

Rauret, G., Rubio, R., Lopezsanchez, J.F., 1989. Optimization of tessier procedure for metal solid speciation in river sediments. Int. J. Environ. Anal. Chem. 36, 69–83.

Ravel, B., Newville, M., 2005. ATHENA, ARTEMIS, HEPHAESTUS: data analysis for X-ray absorption spectroscopy using IFEFFIT. J. Synchrotron Radiat. 12, 537–541.

Reese, R.N., White, C.A., Winge, D.R., 1992. Cadmium-sulfide crystallites in Cd-(gammaEC)(n)G peptide complexes from tomato. Plant Physiol. 98, 225–229.

Rodrigues-Filho, U.P., Vaz Jr, S., Felicissimo, M.P., Scarpellini, M., Cardoso, D.R., Vinhas, R.C.J., Landers, R., Schneider, J.F., Mcgarvey, B.R., Andersen, M.L., 2005. Heterometallic manganese/zinc-phytate complex as a model compound for metal storage in wheat grains. J. Inorg. Biochem. 99, 1973–1982.

Rusinowski, S., Krzyzak, J., Clifton-Brown, J., Jensen, E., Mos, M., Webster, R., Sitko, K., Pogrzeba, M., 2019a. New Miscanthus hybrids cultivated at a Polish metal-contaminated site demonstrate high stomatal regulation and reduced shoot Pb and Cd concentrations. Environ. Pollut. 252, 1377–1387.

Rusinowski, S., Krzyzak, J., Sitko, K., Kalaji, H.M., Jensen, E., Pogrzeba, M., 2019b. Cultivation of C4 perennial energy grasses on heavy metal contaminated arable land: Impact on soil, biomass, and photosynthetic traits. Environ. Pollut. 250, 300–311.

Salt, D.E., Prince, R.C., Baker, A.J.M., Raskin, I., Pickering, I.J., 1999. Zinc ligands in the metal hyperaccumulator Thlaspi caerulescens as determined using X-ray absorption spectroscopy. Environ. Sci. Technol. 33, 713–717.

Sarret, G., Saumitou-Laprade, P., Bert, V., Proux, O., Hazemann, J.-L., Traverse, A., Marcus, M.A., Manceau, A., 2002. Forms of zinc accumulated in the hyperaccumulator Arabidopsis halleri. Plant Physiol. 130, 1815–1826.

Sarret, G., Willems, G., Isaure, M.P., Marcus, M.A., Fakra, S.C., Frerot, H., Pairis, S., Geoffroy, N., Manceau, A., Saumitou-Laprade, P., 2009. Zinc distribution and speciation in Arabidopsis halleri x Arabidopsis lyrata progenies presenting various zinc accumulation capacities. New Phytol. 184, 581–595.

Sharma, A., Patni, B., Shankhdhar, D., Shankhdhar, S.C., 2013. Zinc – an indispensable micronutrient. Physiol. Mol. Biol. Plants 19, 11–20.

Singh, K., 1986. The critical level of zinc in soil and plant for predicting response of cluster bean to zinc fertilization. Plant Soil 94, 285–288.

Steffens, J.C., 1990. The heavy metal-binding peptides of plants. Annu. Rev. Plant Physiol. Plant Mol. Biol. 41, 553–575.

Suganya, A., Saravanan, A., Manivannan, N., 2020. Role of zinc nutrition for increasing zinc availability, uptake, yield, and quality of maize (Zea mays L.) grains: an overview. Commun. Soil Sci. Plant Anal. 51, 2001–2021.

Terravesta 2018. Soil Analysis Bytom 20.09.16. Unpublished.

Terzano, R., Al Chami, Z., Vekemans, B., Janssens, K., Miano, T., Ruggiero, P., 2008. Zinc distribution and speciation within rocket plants (Eruca vesicaria L. Cavalieri) grown on a polluted soil amended with compost as determined by XRF microtomography and micro-XANES. J. Agric. Food Chem. 56, 3222–3231.

Terzano, R., Mimmo, T., Vekemans, B., Vincze, L., Falkenberg, G., Tomasi, N., Schnell Ramos, M., Pinton, R., Cesco, S., 2013. Iron (Fe) speciation in xylem sap by XANES at a high brilliant synchrotron X-ray source: opportunities and limitations. Anal. Bioanal. Chem. 405 (16), 5411–5419.

Tessier, A., Campbell, P.G.C., Bisson, M., 1979. Sequential extraction procedure for the speciation of particulate trace-metals. Anal. Chem. 51, 844–851.

Thomas, S.A., Mishra, B., Myneni, S.C.B., 2019. High energy resolution-X-ray absorption near edge structure spectroscopy reveals Zn ligation in whole cell bacteria. J. Phys. Chem. Lett. 10, 2585–2592.

Valeev, R.G., Beltukov, A.N., Gilmutdinov, F.Z., Romanov, É., Deev, A.N., Kriventsov, V. V., Mezentsev, N.A., Chukavin, A.I., 2011. EXAFS spectroscopy study of the atomic structure of ZnS nanocomposite thin films. J. Struct. Chem. 52, 181–185.

Van Der Weijde, T., Kiesel, A., Iqbal, Y., Muylle, H., Dolstra, O., Visser, R.G.F., Lewandowski, I., Trindade, L.M., 2017. Evaluation of Miscanthus sinensis biomass quality as feedstock for conversion into different bioenergy products. Glob. Change Biol. Bioenergy 9, 176–190.

Venkatesh, M.S., Hazra, K.K., Ghosh, P.K., 2014. Critical tissue concentration of zinc in short duration mungbean (Vigna radiata). Indian J. Agric. Sci. 84, 892–894.

Verkleij, J.A.C., Koevoets, P.L.M., Blake-Kalff, M.M.A., Chardonnens, A.N., 1998. Evidence for an important role of the tonoplast in the mechanism of naturally selected zinc tolerance in Silene vulgaris. J. Plant Physiol. 153, 188–191.

Vijayan, P., Willick, I.R., Lahlali, R., Karunakaran, C., Tanino, K.K., 2015. Synchrotron radiation sheds fresh light on plant research: the use of powerful techniques to probe structure and composition of plants. Plant Cell Physiol. 56, 1252–1263.

Wanat, N., Austruy, A., Joussein, E., Soubrand, M., Hitmi, A., Gauthier-Moussard, C., Lenain, J.F., Vernay, P., Munch, J.C., Pichon, M., 2013. Potentials of Miscanthus x giganteus grown on highly contaminated Technosols. J. Geochem. Explor. 126, 78–84.

Wang, Y.H., Zhan, M.G., Zhu, H.X., Guo, S.J., Wang, W.S., Xue, B.M., 2012. Distribution and accumulation of metals in soils and plant from a lead-zinc mineland in Guangxi, South China. Bull. Environ. Contam. Toxicol. 88, 198–203.

Weik, M., Ravelli, R.B.G., Kryger, G., Mcsweeney, S., Raves, M.L., Harel, M., Gros, P., Silman, I., Kroon, J., Sussman, J.L., 2000. Specific chemical and structural damage to proteins produced by synchrotron radiation. Proc. Natl. Acad. Sci. 97 (2), 623–628.

Zhao, F.J., Moore, K.L., Lombi, E., Zhu, Y.G., 2014. Imaging element distribution and speciation in plant cells. Trends Plant Sci. 19, 183–192.